J. Fluid Mech. (1990), *vol.* 210, *pp.* 475–500
Printed in Great Britain

Small-scale transition in a plane mixing layer

By LEIN-SAING HUANG† AND CHIH-MING HO
Department of Aerospace Engineering, University of Southern California, Los Angeles, CA 90089, USA

(Received 11 January 1989 and in revised form 22 June 1989)

An experimental study was conducted to investigate the generation process of random small-scale turbulence in an originally laminar mixing layer. The evolutions of the two types of deterministic structures, the spanwise and streamwise vortices, were first clarified in order to determine their roles in the transition process. A scaling rule for the streamwise distance from the trailing edge of the splitter plate to the vortex merging position was found for various velocity ratios. After this streamwise lengthscale was determined, it became clear that the spanwise wavelength of the streamwise vortices doubled after the merging of the spanwise structures which nominally doubled streamwise wavelengths. The most interesting finding was that the random small-scale eddies were produced by the interactions between the merging spanwise structures and the streamwise vortices.

1. Introduction

The mixing of fluids between two streams with different velocities is the major problem for mixing-layer research. The fluids in the two streams are first entrained into the shear region either by the merging of the coherent structures (Brown & Roshko 1974; Winant & Browand 1974) or by the three-dimensional evolution of asymmetric vortices (Ho & Gutmark 1987). Fine-scale mixing of the fluids then takes place at the convoluted interfaces. In a shear layer with originally laminar flow, the mixing initially occurs at the folds of the spanwise structures and the streamwise vortices (Bernal & Roshko 1986) and increases to a much higher level at a certain streamwise region. Konrad (1976) observed the sudden increase of mixing in this region and called it mixing transition, as it is related to the generation of fine turbulent eddies (Sato 1960; Bradshaw 1966; Liu & Merkine 1976; Liu 1986).

For technical applications, it is advantageous to be able to control the mixing process (Ho & Huerre 1984; Wygnanski & Petersen 1985). During the past few years, several effective techniques have been developed to manipulate the evolution of the coherent structures such that the entrainment of fluids into the shear layer is altered. For example, by applying active perturbations near the origin of the shear layer (Ho & Huang 1982; Oster & Wygnanski 1982; Fiedler & Mensing 1985; Lee & Reynolds 1985), the spreading of the shear layer can be either suppressed or enhanced. Ho & Gutmark (1987) found a passive method to increase the entrainment by simply using an elliptic jet with a small aspect ratio. These methods mainly vary the amount of fluid engulfed into the shear layer and do not directly influence the small-scale mixing.

For the purpose of being able to control the fine-scale mixing, we first must understand how the small random eddies in an originally laminar mixing layer are

† Present address: NASA-Langley Research Center, Hampton, VA 23665, USA.

generated. In order to locate where the small eddies are first found in relation to the coherent structures, the lengthscales characterizing the evolutions of the streamwise and spanwise structures are identified. It then becomes clear that the small eddies are produced by the interaction of these two types of deterministic structures. Finally, the time-averaged turbulence properties are summarized in this paper.

2. Experimental facility and technique

2.1. *Wind tunnel*

The experiments were conducted in an open loop wind tunnel. The detailed documentation of the wind tunnel and flow properties can be found in the paper by Browand & Latigo (1979) and Huang (1985). The stilling section of the wind tunnel is divided into two independent sections by a splitter plate. At the beginning of the test section, each stream has a cross-section of 30.5 cm high and 91.4 cm wide. In order to obtain different velocities in the two streams, a series of cloth meshes were added to the upper half of the settling section inlet to produce the required pressure drop for a desired velocity difference. The velocity ratio is defined as $R = \Delta U/\bar{U}$ where ΔU is $(U_1 - U_2)$ and $\bar{U}$ is the average velocity, $\frac{1}{2}(U_1 + U_2)$. For vortex merging and transition studies, velocity ratios were varied from 0.4 to 1.0. Most of the experiments were performed at $R = 0.69$, the high speed stream, U_1, was 19.8 m/s and the low speed stream, U_2, was 3.63 m/s. The flow was uniform across the span within 0.25% of the maximum velocity in either stream. The free-stream turbulence intensity, $u'/\Delta U$, was approximately equal to 0.3% in the low-speed stream and less than 0.1% in the high-speed stream. The boundary layers at the trailing edge of the splitter plate were laminar for both streams.

2.2. *Acoustic excitation*

Acoustic waves were applied to excite the shear layer. A unique design was used to introduce the sound into the flow. The last section of the splitter plate was a specially manufactured steel plate (Huang 1985), where milled inside was a wedge-shaped chamber. The acoustic waves were produced by a loudspeaker placed outside the wind tunnel and guided through a tube into the tip of the chamber. The waves emitted from a 0.5 mm wide spanwise slit into the low-speed side. The slit was located 8 cm upstream from the trailing edge. The excitation wave modulated the boundary layer on the low-speed side.

Two combined frequencies, the initial instability frequency, f_0, and the subharmonic, $\frac{1}{2}f_0$, with the same amplitude were selected to perturb the flow. A digital circuit designed by D. Plocher was used to generate the forcing signal. Through a power amplifier, the forcing signal drove the loudspeaker. The amplitude and the phase of the forcing across the span was checked using a $\frac{1}{8}$ in condenser microphone (Bruel & Kjaer type 4138) in the quiescent environment and they were uniform over 80% of the span (Huang 1985).

2.3. *Instruments and data processing*

The velocity measurements were obtained with an x-wire probe. The constant temperature hot-wire anemometer had a flat frequency response up to 30 kHz. The wire used was made of 10% rhodium–platinum wire, 0.0025 mm in diameter and about 1.5 mm in length. A generalized polynomial form for the two velocity components u and v and the wire output voltages was assumed. The ten coefficients were determined using a least-squares method to fit 30 data points of known

velocities and flow directions. The x-wire output was first recorded on a Hewlett Packard 14 channel tape recorder (type 3955A) and then digitized by a PDP 11/55 minicomputer (12 bit A/D converter).

The fast Fourier transform (FFT) technique was used to compute the velocity power spectra. The conditional sampling technique was also employed to define the contour of the vortical structures. The maximum entropy method (Burg 1967; Chen & Stegen 1974) was applied to estimate the wavelength of streamwise vortices. This method is powerful in determining the peak frequency when only a short piece of record is available.

While the streamwise vorticity was calculated from the transverse velocity distributions, the running median method proposed by Tukey (1974) was used to smooth small-amplitude fluctuations caused by measurement inaccuracy. The method still retained the velocity jump which represented the vorticity. In the phase averaged case, the forcing signal was used as a phase reference. The error caused by the phase jitter was not significant, because the measuring station is still upstream from the phase de-correlation region (Zohar, Foss & Ho 1987). The inaccuracy of the vorticity measurements involved the calibration error of the velocity, the spatial resolution of the probe location and the phase jitter. The uncertainty of measuring one component of the streamwise vorticity was estimated to be about 10%.

3. Evolution of the spanwise structures

3.1. *The amplification of stability waves and vortex merging*

In a forced mixing-layer experiment performed in a low-Reynolds-number water channel, Ho & Huang (1982) identified the relationship between stability waves and vortices; the saturation of the fundamental corresponded to the roll-up of the vortex and the saturation of the subharmonic corresponded to the vortex merging. In this study, we performed the same measurement in an unforced flow with a Reynolds number about two orders of magnitude higher than the 1982 experiment. At each streamwise location, spectra of the streamwise velocity fluctuations were measured at about twenty stations across the shear layer. The narrow band energy contents, $E(u^*(f))$, at the fundamental and the subharmonic were integrated along the transverse direction and offered an overall measure of the energy at the specific stability frequency. $E(u^*(f))$ is defined as

$$E[u^*(f)] = \frac{1}{2\theta_0}\int_{-\infty}^{+\infty}\left(\frac{u^*(f)}{\Delta U}\right)^2 \mathrm{d}y \quad (u^* = u, v \text{ or } w), \tag{1}$$

where θ_0 is the initial momentum thickness of the high-speed side (see §6.1). The streamwise variations of $E[u(f)]$ are plotted in figure 1. The maximum level of the subharmonic occurred at about twice the distance downstream from the region where the fundamental saturated. The same measurement was carried out for the forced condition. The stability waves in the low-level forced mixing layer also reached their maximum value at $x = 4.5$ cm (figure 1). The phase averaged vorticity contours (Huang 1985) did show that the initial vortex rolled up near $x = 4.5$ cm and the neighbouring vortices coalesced around $x = 9$ cm. This exercise again established the relationship of the stability waves and the vortex motion in unforced and forced high-Reynolds-number flows.

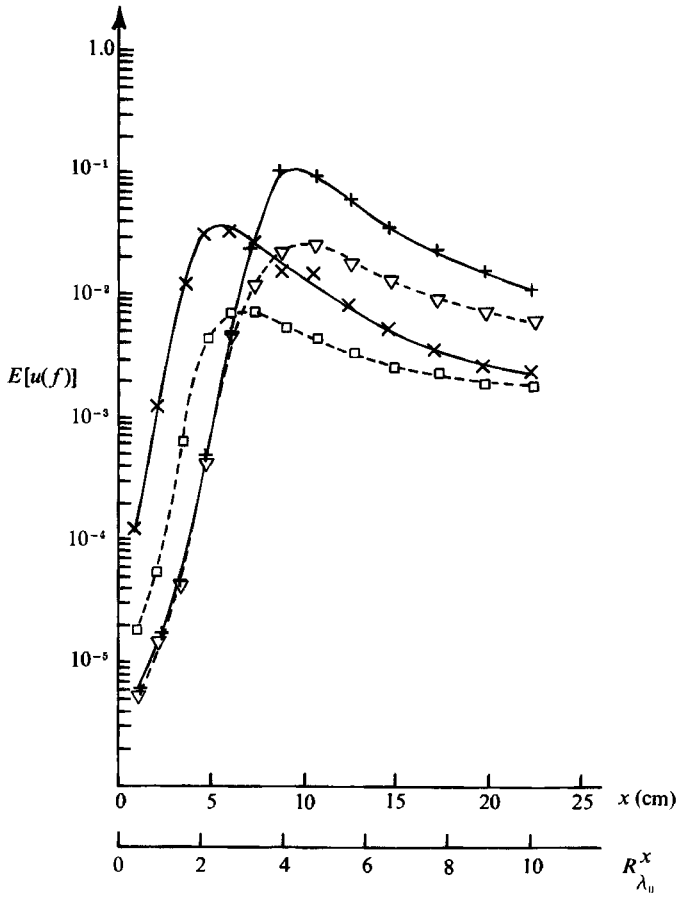

FIGURE 1. Energy content of $u(f)$ *vs.* streamwise distance. For the forced case: ×, 750 Hz $= f_0$; +, 375 Hz $= \frac{1}{2}f_0$. For the unforced case: □, 750 Hz; ▽, 375 Hz. $\lambda_0 = 1.56$ cm.

3.2. *The streamwise lengthscale*

Vortical structures play a dominant role in the development of shear layers. They are responsible for mass entrainment (Winant & Browand 1974; Riley & Metcalfe 1980; Ho & Huang 1982) and momentum transfer (Browand & Ho 1983). If a non-dimensional lengthscale corresponding to the streamwise evolution of the vortices, i.e. roll-up and coalescence, can be identified, it will be useful in understanding the dynamics of the flow. Both the roll-up and the coalescence of the vortices take place in a region, not at a single point. For convenience, we have suggested using the location where the stability waves reach their maximum level as the vortex merging position (Ho & Huang 1982).

The vortex merging position varies with the operating conditions of the mixing layer. The important variables are the free-stream velocities, U_1 and U_2, and the initial instability frequency, f_0. In order to determine the scaling rule, the vortex merging positions need to be measured at many operating conditions. However, it is very tedious to obtain the stability amplification curves (figure 1) or the vorticity contours. We bypassed this enormous data taking task by measuring the passage frequency of the vortices. A hot-wire probe was placed at the low-speed side and at four local momentum thicknesses away from the centreline of the mixing layer. The

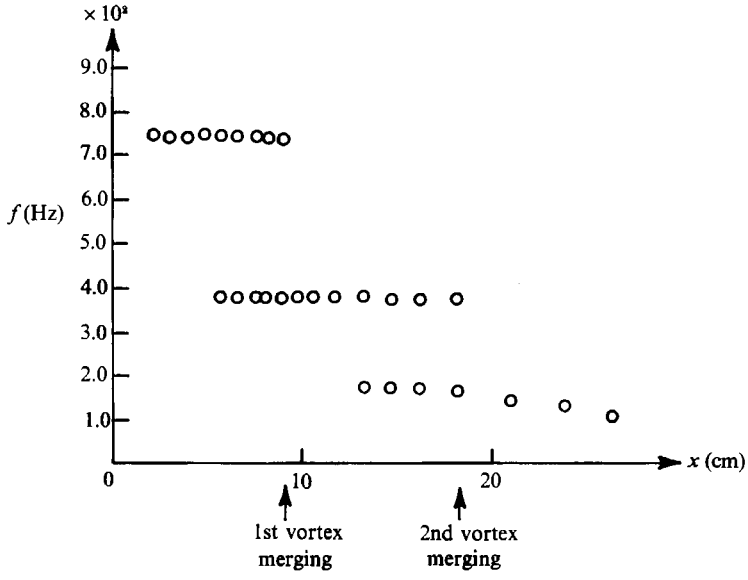

FIGURE 2. Variation of the passage frequency with streamwise distance for the unforced case: $R = 0.69$, $\bar{U} = 11.71$ m/s. $\lambda_0 = 1.56$ cm.

probe was outside the shear region and sensed the velocity fluctuations induced by the coherent structures but was not contaminated by the small-scale turbulence. Very near the trailing edge of the splitter plate, the velocity spectrum had a sharp peak which was the most amplified frequency. When the probe was moved downstream, the first subharmonic emerged from the noise. The subharmonic spectral intensity grew while the fundamental peak decayed with the streamwise distance. When the spectral intensity of the fundamental dropped one decade below that of the first subharmonic at $x = 4.5$ cm, the fundamental was not plotted. The same sequence was observed for the first and second subharmonics. The peak frequencies are shown in figure 2. After the first subharmonic dropping from the diagram at $x = 9$ cm, the spectrum became broadband. The peak of the spectrum decreased continuously with the distance. Comparison of figure 1 and figure 2 indicates that the fundamental ended at the first vortex merging position. After two vortices coalesce, it is reasonable to expect that the induced velocity of each single vortex is greatly reduced. So the end of the first subharmonic corresponds to the second vortex merging position. By applying this much simpler technique, the vortex merging positions for various velocity combinations were studied. For the purpose of establishing a streamwise lengthscale for the merging of coherent structures, we grouped the operating variables, U_1, U_2 and f_0, into two parameters. One is the velocity ratio, $R = \Delta U/\bar{U}$, which is a measure of the ratio between the rates of deformation and advection. The other is the initial instability wavelength, $\lambda_0 = \bar{U}/f_0$, which is a measure of the distance between the vortices. With the measured values of the vortex merging positions, x_m, and the two parameters, the first vortex merging position was identified to be at $x_m^* = Rx_m/\lambda_0 = 4$ and the second one at $x_m^* = 8$ (figure 3). The finding of this lengthscale enabled us to relate the evolution of the streamwise vortices and the small-scale transition to the coalescence of the spanwise structures. The same type of normalization was used for the streamwise coordinate, x, as $x^* = Rx/\lambda_0$. According to the stability analysis (Monkewitz &

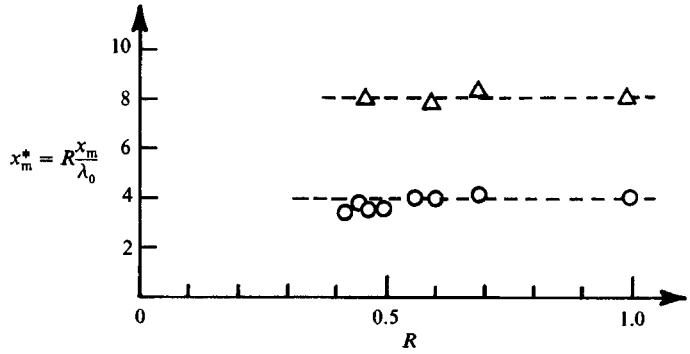

FIGURE 3. Non-dimensional vortex merging position *vs.* velocity ratio.

R	$\bar{U}$ (m/s)	λ_0 (cm)
1.00	12.0	0.65
0.69	10.2	1.26
0.60	8.10	2.02
0.56	13.5	1.41
0.50	10.2	1.75
0.48	13.5	1.57
0.45	10.2	1.81
0.42	6.90	2.09

Huerre 1982), the ratio between the initial momentum thickness and the most amplified streamwise wavelength is almost constant, 0.034, for various velocity ratios. In unforced flows, λ_0 in the normalized x, x^*, can be replaced by the initial momentum thickness and a proportional constant. When the flow is forced, however, the streamwise wavelength of perturbed coherent structures, λ_0, instead of the initial momentum thickness is the relevant lengthscale and should be used in normalization.

4. Evolution of the streamwise vortices

4.1. *Initial development of the secondary structures*

In a plane mixing layer, the flow is not two-dimensional. Miksad (1972) reported non-uniformity in the spanwise direction. Konrad (1976) observed streamwise streaks. It was then identified that these streaks were counter-rotating vortex pairs (Breidenthal 1981; Bernal 1981; Lasheras, Cho & Maxworthy 1986; Nygaard & Glezer 1988). Through elaborate visualizations, Bernal (1981) reconstructed the spatial configuration of the secondary vortices which are interlaced between the adjacent spanwise structures.

In a natural mixing layer without artificial forcing, we investigated the initial stage of the vortices through the velocity fluctuations near the origin of the shear flow. In the region near the trailing edge of the splitter plate, $x^* \ll 4$, the fluctuating velocities of a laminar shear flow are derived from the development of the deterministic structures. According to the orientations of these structures, the amplifications of u and v are associated with the roll-up of the spanwise structures, whereas v and w grow with the formation of the streamwise vortices. Therefore, the spanwise velocity fluctuations, w, indicate the development of the streamwise vortices. The fluctuations are modulated by the passage of the spanwise structures. Hence the spectral content of $w, E[w(f)]$, is dominated by a peak at the most

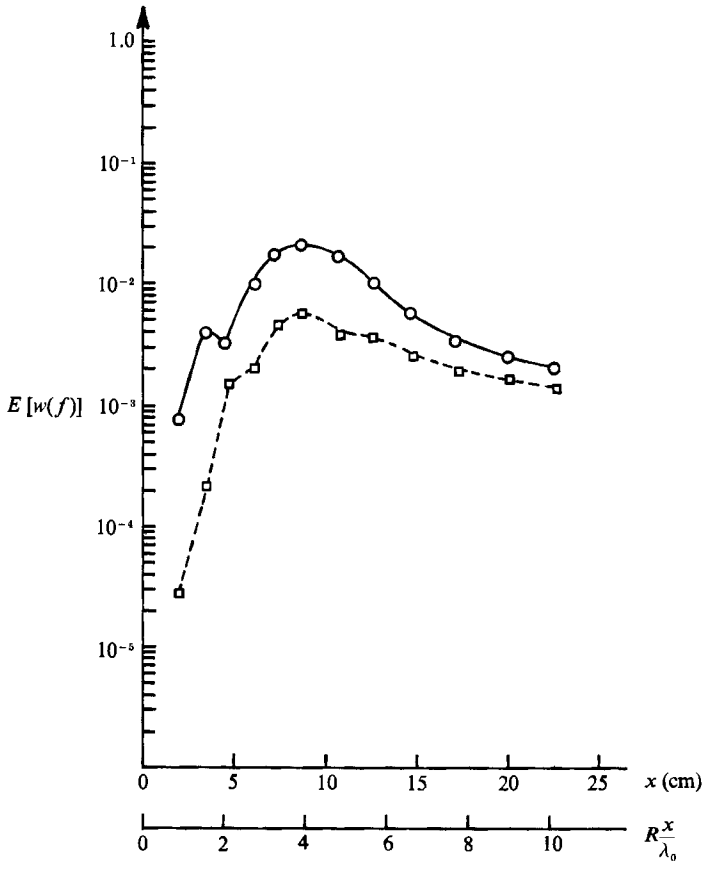

FIGURE 4. Energy content of $w(f)$ *vs.* streamwise distance. for the forced case: ○, 750 Hz $= f_0$. For the unforced case: □, 750 Hz.

amplified frequency in the initial region of the mixing layer. $E[w(f)]$ is defined in equation (1) and its variation with distance is shown in figure 4. $E[w(f)]$ can be detected close to the trailing edge of the splitter plate, $x^* < 1$, and its magnitude amplifies exponentially with distance. Apparently, the secondary vortices develop together with the spanwise structures from the very beginning of the mixing layer.

4.2. *The spanwise distribution of mean velocity profiles*

The time-averaged streamwise velocity was measured along the spanwise direction. A long average time equalling two thousand vortex passage periods was used. The spanwise profiles (figure 5) were measured at the constant transverse locations where $y/\theta = 0$. These profiles were not straight lines, instead they had clear wavy patterns. These patterns were caused by the streamwise counter-rotating vortex pairs. The vortices transferred the high- and low-speed fluids in the two streams across the interface and produced the wavy velocity profiles. Since these velocity distributions were obtained by a long time average, the existence of the wavy pattern implied that the streamwise vortices were localized in the wind tunnel. This result confirmed the finding by Jimenez (1983). As a matter of fact, we repeated the same measurements two months after taking the first set of data, and the peaks and valleys in the two profiles still matched.

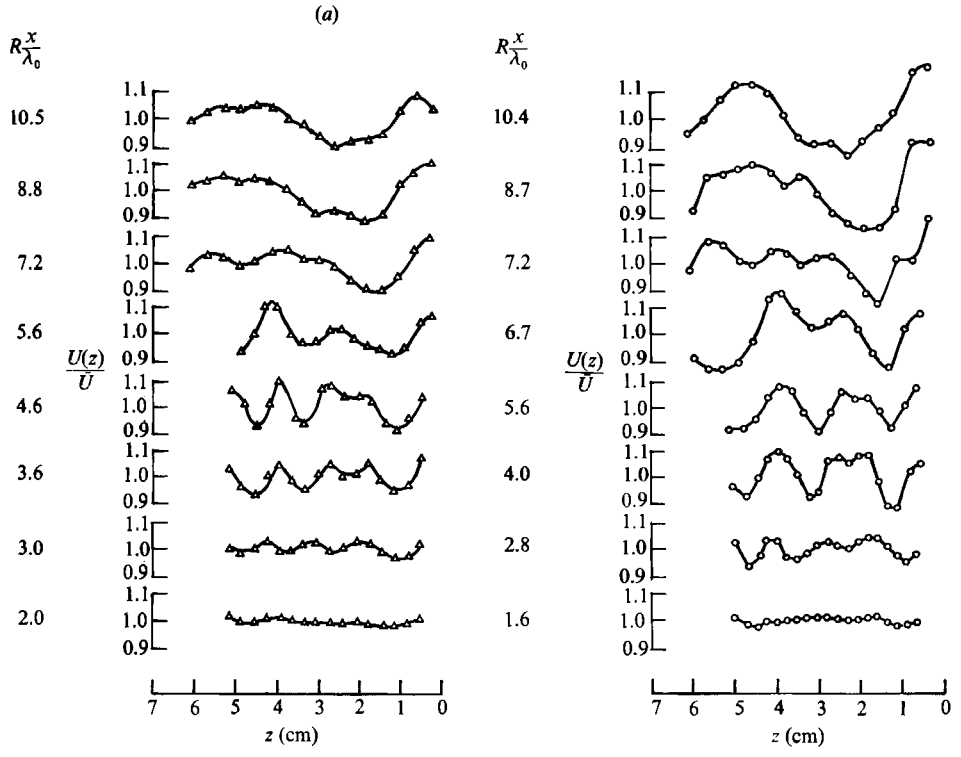

FIGURE 5. Spanwise longitudinal mean velocity distributions *vs.* streamwise distance. (*a*) The spanwise unforced case. (*b*) The spanwise forced case.

We also applied periodic disturbances along the trailing edge of the splitter plate. They were made of narrow Scotch tape blocks 3 mm wide, as thick as the boundary layer and separated by one spanwise wavelength of the streamwise vortices. Based upon the velocity profiles of the forced case (figure 5*b*), the forcing could make the vortices only slightly more regular around the first merging region, $x^* = 4$. At this high-Reynolds-number mixing layer, the three-dimensional forcing was not effective. For the rest of the experiment, no three-dimensional forcing was applied to the streamwise vortices.

The deviation of the local mean velocity from the average speed, $\bar{U}$, increased with streamwise direction. A r.m.s. value defined as

$$U_z = \left[\frac{1}{z_1 - z_2}\int_{z_2}^{z_1}\left(\frac{U(z)}{\bar{U}} - 1\right)^2 \mathrm{d}z\right]^{\frac{1}{2}} \tag{2}$$

was used as an estimate of the cross-stream fluid transfer caused by the secondary vortices. U_z for the unforced case is shown in figure 6. Upstream from the roll-up region of the spanwise structures, the deviation was small compared with the average speed and increased after $x^* = 2$.

An interesting feature can be observed in figure 6. The amplitude of the velocity deviation decayed slightly near the first and second vortex merging regions. This result indicated that the vortex merging process suppressed the activity of the streamwise vortices and made the mixing layer more two-dimensional. A similar feature can be observed in figure 4. The growth of $E[w(f)]$ also decayed near the

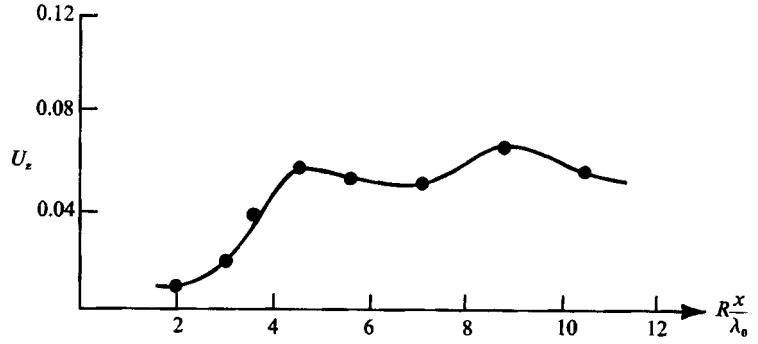

FIGURE 6. Root mean square deviation of velocity from local average velocity *vs.* streamwise distance for the spanwise unforced case.

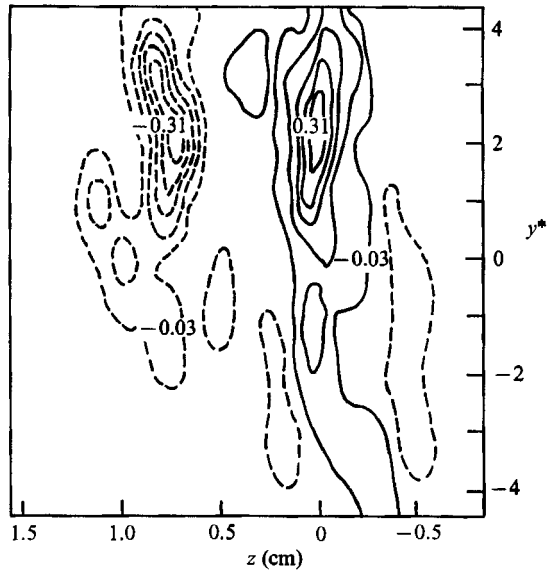

FIGURE 7. Contours of constant $\partial V(y,z)/\partial z$ at $x^* = 2.0$, normalized by maximum $\partial U/\partial y = 3250\ \mathrm{s}^{-1}$. The solid lines are contours of positive streamwise vorticity and the dotted lines are negative streamwise vorticity. The contours are incremented by 0.07. $y^* = y/\theta$, θ is the local momentum thickness.

formation of the spanwise structures, $x^* = 2$, and after the first vortex merging. The reduction of three-dimensional motion around the saturation of the fundamental has been suggested by numerical studies (Corcos & Lin 1984; Metcalfe *et al.* 1987). In the simulation, the stretching in the braid which intensified the streamwise vortices was observed to reduce its level near the saturation of the fundamental. Hence, the growth of the three-dimensional secondary structures was slowed down. In experiment, the data further showed that the similar phenomenon occurred in the process of vortex merging.

4.3. *Vorticity of the secondary structures*

The streamwise vorticity was measured with a x-wire probe to survey the velocity components at two hundred stations in a plane normal to the mean flow direction. This area covered about one and a half wavelengths of the streamwise vortices in the

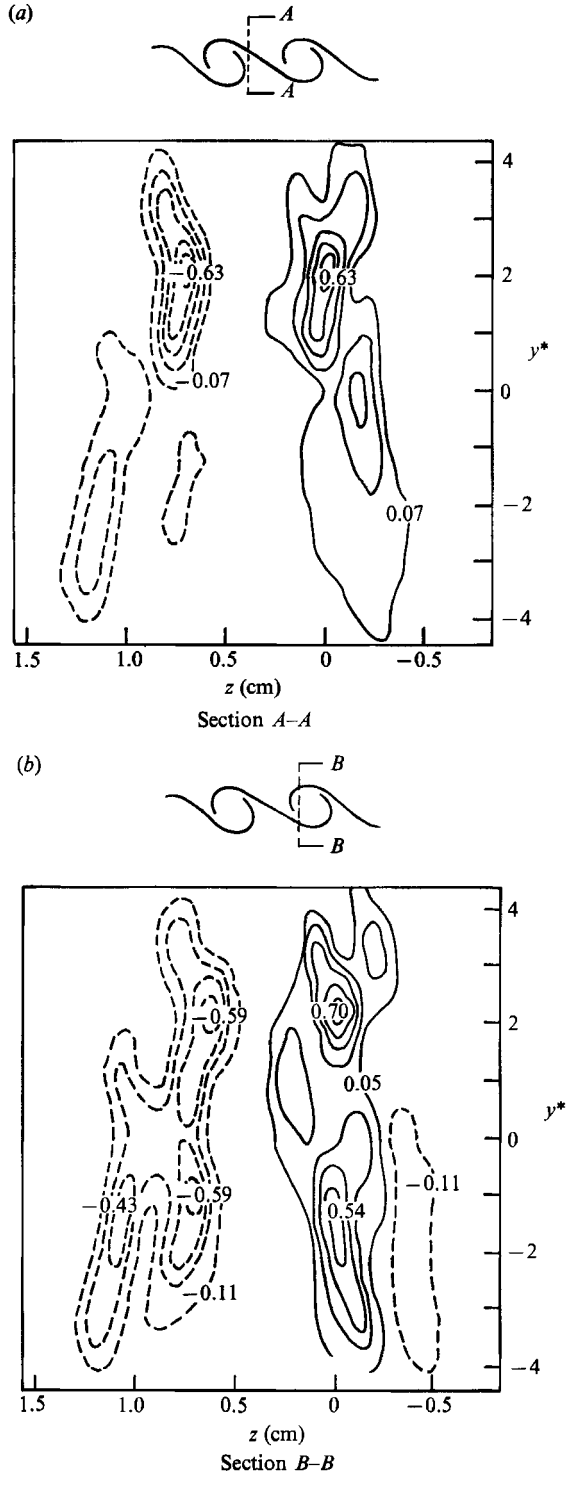

FIGURE 8. Contours of constant $\langle \partial V(y,z,t)\rangle/\partial z$ in a (y,z)-plane at $x^* = 2.0$ normalized by maximum $\partial U/\partial y = 3250\ \mathrm{s}^{-1}$; ——, positive, – – – – – –, negative. (*a*) The sampling plane passes the braid. The contours are incremented by 0.14. (*b*) The sampling plane passes the core. The contours are incremented by 0.16.

spanwise direction and eight momentum thickness of the mixing layer in the transverse direction. The streamwise location was chosen at $x^* = 2$, where the spanwise structures had just rolled up. The streamwise vorticity is, $\Omega_x = \partial V/\partial z - \partial W/\partial y$. In principle, V and W can be obtained by placing the x-wire probe in two orientations and the value of Ω_x can then be calculated. However, the accuracy is greatly decreased while several steps of subtraction are taking place. In order to avoid this problem, we only measured one component of the vorticity, $\Omega_{x'} = \partial V/\partial z$, which still could reveal the spatial structure of the streamwise vortices and offer an estimate of the streamwise vorticity. Figure 7 shows the time averaged $\Omega_{x'}$ and its value is normalized by the maximum $\partial U/\partial y$ obtained at $z = 0$. The data indicated that the counter-rotating streamwise vortex pair had already formed at the roll-up position of the large structures. The streamwise vorticity was fairly strong and was about one-third that of the spanwise structures.

The two-dimensional acoustic forcing was applied through the thin slit near the trailing edge of the splitter plate to organize the spanwise structures. The forcing signal also served as a phase reference for signal processing. The phase-averaged vorticity contours are presented in figure 8. By applying different time delays, we can obtain the streamwise vorticity contours in a plane normal to the free stream and at locations passing the braid or the core of the spanwise structures. When the plane cuts through the braid (figure 8*a*), there are two counter-rotating vortex cores. Four vortex cores were observed in figure 8(*b*), as the sampling plane passes the spanwise structure. This set of data provided a quantitative base for supporting the streamwise vortex morphology constructed from visualization experiments (Bernal 1981; Bernal & Roshko 1986). The maximum vorticity of the phase-averaged value was twice as large as the time-averaged streamwise vorticity and was almost equal to the maximum $\partial U/\partial y$. These strong vortices produced large mean velocity perturbations along the span; more than 10% of the average speed has been detected (figure 5).

4.4. *Adjustment of the spanwise lengthscale*

The streamwise distance between the spanwise structures doubles after pairing. From the mean velocity profiles (figure 5), it is clear that the spanwise wavelength of the streamwise vortices also increases with downstream distance. The maximum entropy technique (Burg 1967; Chen & Stegen 1974) was used to determine the wavelength quantitatively. A few examples of the spectra at different downstream locations are shown in figure 9. The spectra had a dominant peak and several lower peaks. Near the origin of the mixing layer, the secondary vortices had short wavelengths. At downstream locations, a longer wavelength developed and became the dominating one (figure 9*b*). This process repeated in regions further downstream (figure 9*c*). The decaying of the vortices with short wavelengths after the adjustment was very slow. The peak of the initial wavelength could be detected from the spectrum even after the second vortex merging (figure 9*c*). This must be the reason why the apparent wavelength kept constant for a long distance in the flow visualizations (Konrad 1976; Bernal & Roshko 1986), however, the dominating spanwise wavelength has increased its value already. When the dominating spanwise wavelength, λ_3, was normalized with the local streamwise wavelength, λ_2, the value started at 1.5 and decreased with distance (figure 10). At the location where the streamwise vortices and the spanwise structures fully formed, $x^* = 2$, the normalized wavelength, λ_3/λ_2, reached an asymptotic value. This value, 2/3, kept constant after vortex merging. It indicated that the wavelength of the streamwise vortices adjusted

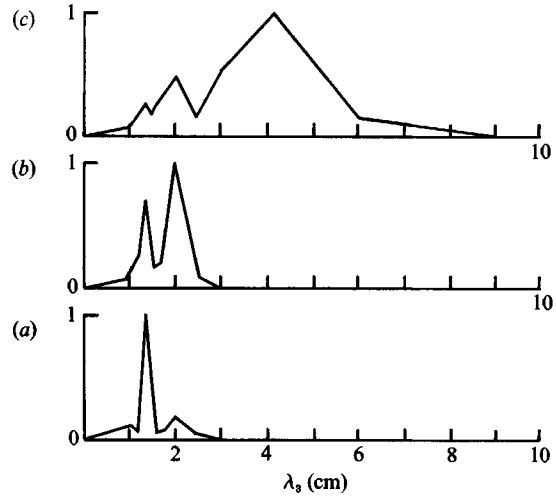

FIGURE 9. Maximum entropy spectra of spanwise mean velocity distribution for the two-dimensional forced case: (*a*) $x^* = 2.8$; (*b*) $x^* = 4.0$; (*c*) $x^* = 10.4$.

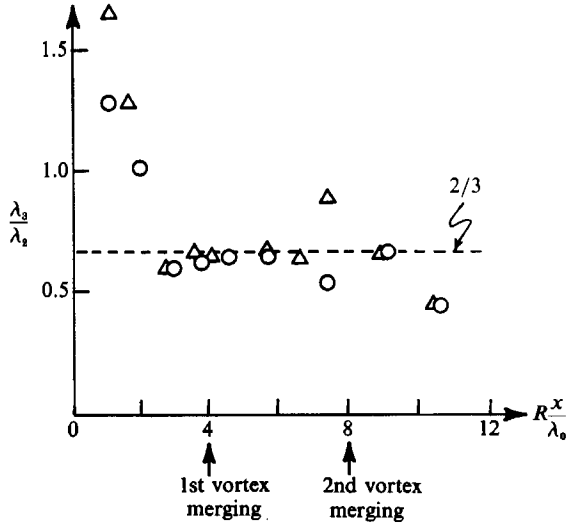

FIGURE 10. Ratio of the three-dimensional wavelength *vs.* the two-dimensional wavelength along the streamwise distance: △, unforced; ○, forced; ------, Pierrehumbert & Widnall (1982).

itself with the varying streamwise wavelength. The ratio was about 2/3 and agreed well with Pierrehumbert & Widnall's (1982) calculations. The adjustment of the spanwise lengthscale with streamwise wavelength indicates that the formation of the streamwise vortices is an instability process. The primary vortices with a certain wavelength will select a preferred spanwise wavelength to support the secondary vortices. When the distance between the primary vortices doubles, the most amplified wavelength in the spanwise direction changes accordingly. In a numerical simulation (Zohar *et al.* 1988), linear broadband disturbances were used as initial conditions of the streamwise vortices, the amplification rates of these perturbations confirmed the adjustment of the most amplified wavelength band after each vortex merging.

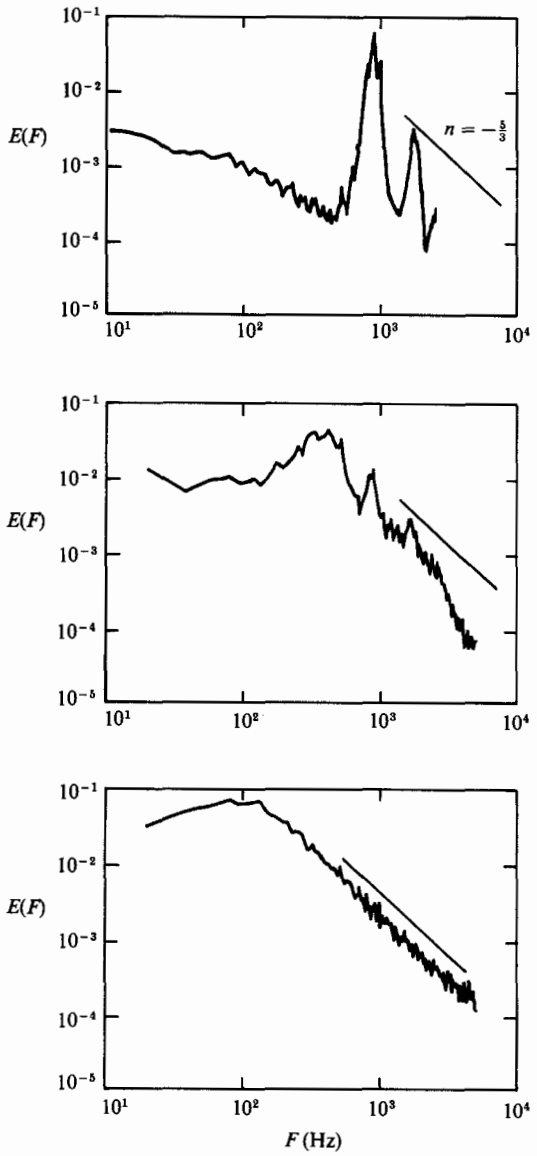

FIGURE 11. Power spectra of longitudinal velocity fluctuation at $y^* = 0$: (*a*) $x^* = 2$; (*b*) $x^* = 5$; (*c*) $x^* = 8$.

5. Generation of random small eddies

5.1. *The role of spanwise structures*

For an initially laminar mixing layer, the spanwise structures and the streamwise structures were deterministic in nature. The flow eventually became turbulent at a certain downstream region, i.e. the random small-scale eddies appear and superimpose on the deterministic structures. In the laminar region, the spectrum had well-defined narrow peaks which represent the most amplified frequency of the instability waves or the structures (figure 11*a*). Further downstream, a roll-off exponent at the frequency range one decade higher than the local vortex passage

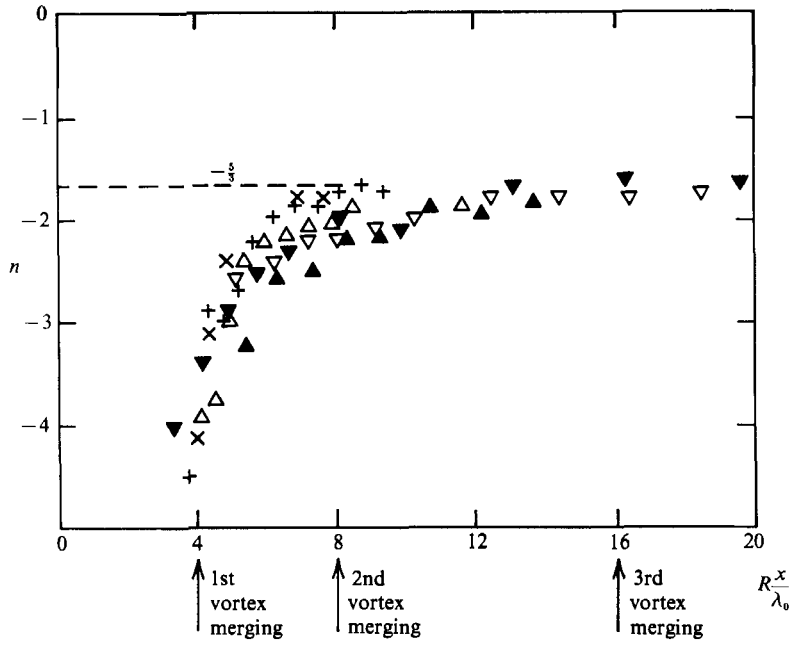

FIGURE 12. Roll-off exponent of power spectra *vs.* non-dimensional streamwise distance in wind tunnel tests. ×, $R = 0.45$, $\bar{U} = 10.2$ m/s; △, $R = 0.50$, $\bar{U} = 10.2$ m/s; +, $R = 0.69$, $\bar{U} = 10.2$ m/s; ▲, $R = 1.00$, $\bar{U} = 12.0$ m/s; ▽, $R = 1.00$, $\bar{U} = 12.5$ m/s (Jimenez *et al.* 1979); ▼, $R = 1.00$, $\bar{U} = 8.2$ m/s (Jimenez *et al.* 1979).

frequency could be defined (figure 11*b*). The roll-off exponent, n, increased its value with streamwise distance and finally reached the asymptotic value of $-\frac{5}{3}$ which showed the establishment of an inertial sub-range by the presence of small eddies (figure 11*c*). Furthermore, it was found that the roll-off exponents were not very sensitive to transverse locations inside the shear region (Jimenez, Martinez-Val & Rebollo 1979). If the roll-off exponent was plotted as a function of streamwise distance, the value started at -4 and increased to $-\frac{5}{3}$ in a short distance (figure 12). This region of abrupt change varied with the operating conditions, i.e. the velocity ratio and the mean velocity. It was interesting to note that the regions of a sudden jump of n could be collapsed into the non-dimensional streamwise distance, $x^* = Rx/\lambda$. Around the first vortex merging region, $x^* = 4$, the roll-off exponent was about 4. This was produced by the folds of the spanwise structures (Lesieur *et al.* 1988). These folds produced structures much smaller than the large spanwise structures, but these small structures were two-dimensional not three-dimensional random eddies. At $x^* = 8$, the asymptotic value of $-\frac{5}{3}$ was reached and the flow became turbulent around this region (Ho & Huerre 1984). This collapse of data was significant because it indicated that the small-scale transition was correlated to the merging of the spanwise coherent structures. In other words, the process of vortex merging shifted energy from the spectral peak to both the high frequency, fine eddies, and the low frequency subharmonic regimes.

5.2. *The role of the Reynolds number*

Coherent structures originate from the inviscid instability and are not Reynolds-number dependent. However, the small eddies cannot exist in low-Reynolds-number

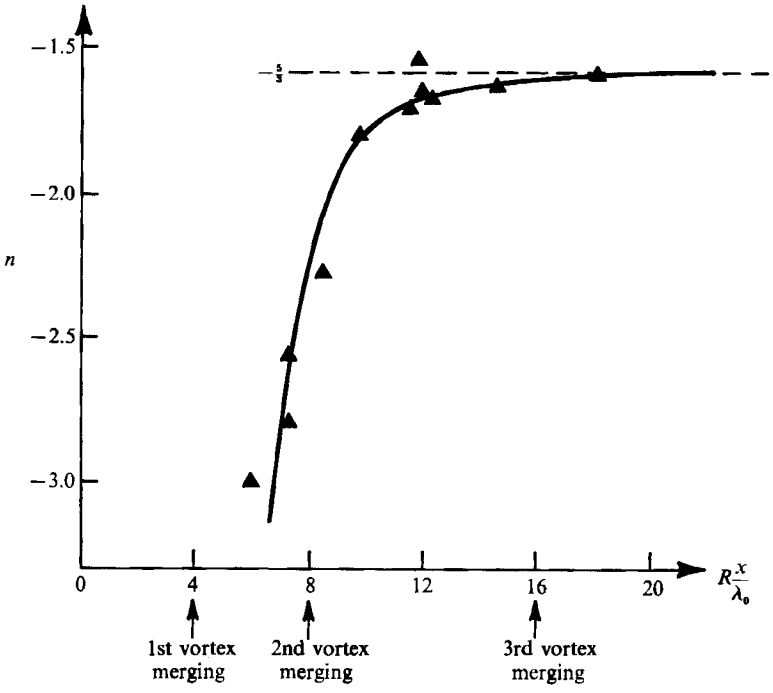

FIGURE 13. Roll-off exponent of power spectra *vs.* non-dimensional streamwise distance in water channel tests, $R = 0.31$ (Jimenez *et al.* 1979).

flows, because the high viscous dissipation will smooth out the sharp velocity gradient and eliminate the fine-scale turbulence. Therefore, the local Reynolds number must be high enough in order to experience the small-scale transition. In the present experiment, the Reynolds number based on the local maximum vorticity thickness, $Re = \bar{U}\delta(x)/\nu$, at $x^* = 8$ varied in a range of 13000–19000. It is clear that there is no definite threshold Reynolds number for transition. The vortex merging will trigger the mixing transition whenever the local Reynolds number is high enough.

In the present wind tunnel test, the Reynolds number based upon the initial vorticity thickness is in the order of 2000 which is about two orders of magnitude higher than that of a typical water channel test. Hence, it is expected that the small-scale transition in water facilities will occur further downstream in order to achieve a high local Reynolds number. As a matter of fact, we rescaled the water channel experiments by Jimenez *et al.* (1979). The sharp rise of the roll-off exponent was still scaled with the vortex merging locations, but was delayed to between the second and third vortex merging regions (figure 13).

5.3. *The role of streamwise vortices*

Very revealing measurements were made at the location of $x^* = 3.85$ where the beginning of the small-scale transition occurred. The flow was not fully contaminated by the random eddies at this point. The measurements were performed by placing five hot-wires in the spanwise direction. Two of them were situated in the cores of the streamwise vortices. The others were located between the streamwise vortices (figure 14). The velocity traces of these three probes were regular and periodic. The velocity

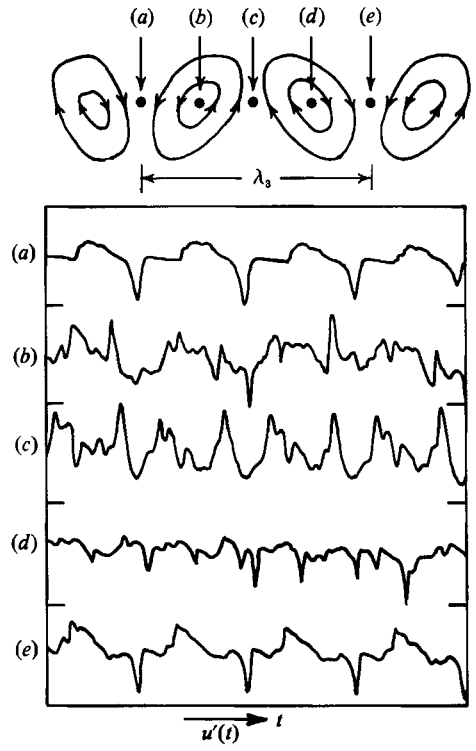

FIGURE 14. Hot-wire traces of u' at five spanwise locations: (*a*) $z = -0.8$ cm; (*b*) $z = -0.2$ cm; (*c*) $z = 0.3$ cm; (*d*) $z = 0.6$ cm; (*e*) $z = 1.2$ cm and $y^* = -1$, $x^* = 3.85$.

traces measured at the cores of the streamwise vortices were distinctly different. High-frequency random velocity fluctuations had been observed. In other words, fine-scale turbulence was first found in the cores of the streamwise vortices at the point where the spanwise structures rolled around and coalesced. Hsiao (1985) found that the high-frequency fluctuations had a preferred frequency which could be associated with a higher-order instability of the streamwise vortices. Robinson & Saffman (1984) found that a vortex subjected to contraction strain field became unstable. Based upon the data (figures 12 and 14), we speculate that the small-scale transition is produced by the strain field of the merging vortices imposed on the streamwise vortices, the strained streamwise vortices were unstable and originated the random fine-scale turbulence.

5.4. *The peak-valley-counting (PVC) technique*

In order to provide a quantitative measure of the small-scale turbulence, we developed a technique to determine the location and the instant of occurrence of the fine-scale velocity fluctuations. The velocity traces consist of low-frequency high-amplitude fluctuations representing the passage of the coherent structures and high-frequency perturbations (figure 15). First we removed the d.c. component and amplified the signal to make sure that the low-amplitude fluctuations stayed above the bit noise of the analogue to digital converter. We then located the local peak and registered the instant by a pulse when the low-frequency portion was negative. If the low-frequency signal was above zero, the instant of occurrence of a local valley was registered by a pulse. By using this method, the local maximum or minimum

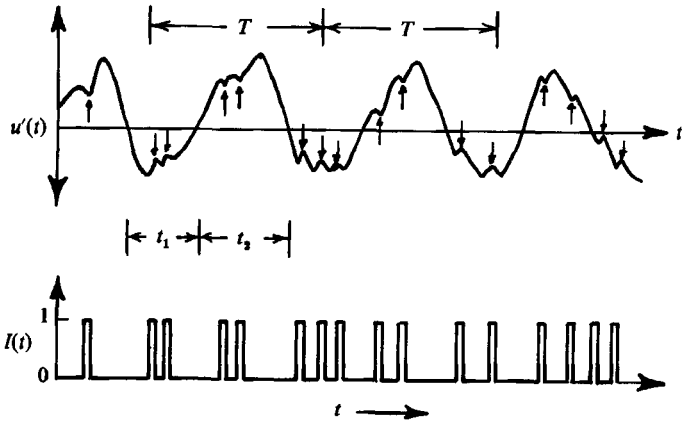

FIGURE 15. Schematic illustration of peak-valley-counting (PVC) method.

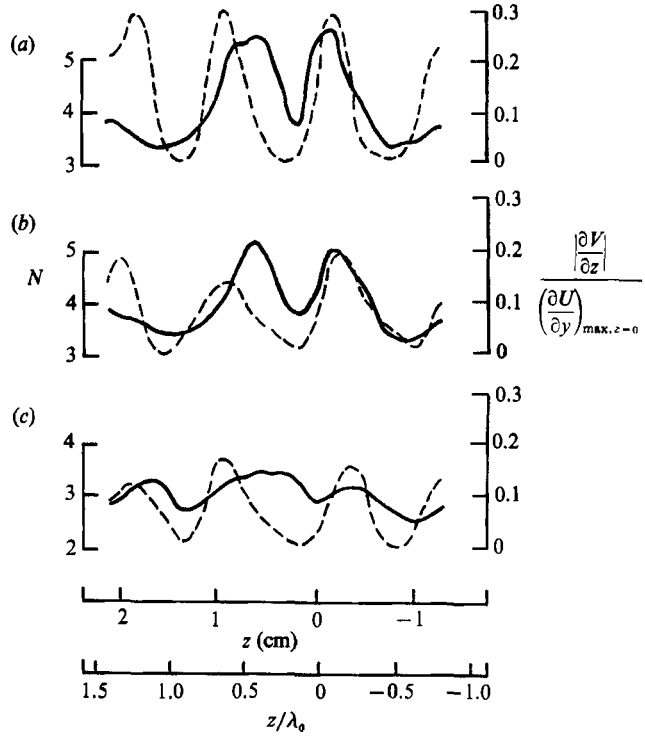

FIGURE 16. Spanwise distribution of N, solid line, and the normalized $|\partial V/\partial z|$, dashed line, at $x^* = 3.85$ and (*a*) $y^* = 1$; (*b*) $y^* = -1$; (*c*) $y^* = -2$.

contributed by the coherent structure was not registered. This was especially important at the region of initial transition, because only a few high-frequency fluctuations occurred during each period of the coherent structures. If the PVC technique was not used, a significant part of the pulses would have been contributed by the passing coherent structures. Further downstream where the small eddies were abundant, the results of the PVC method were not much different from the techniques of locating the local extremes.

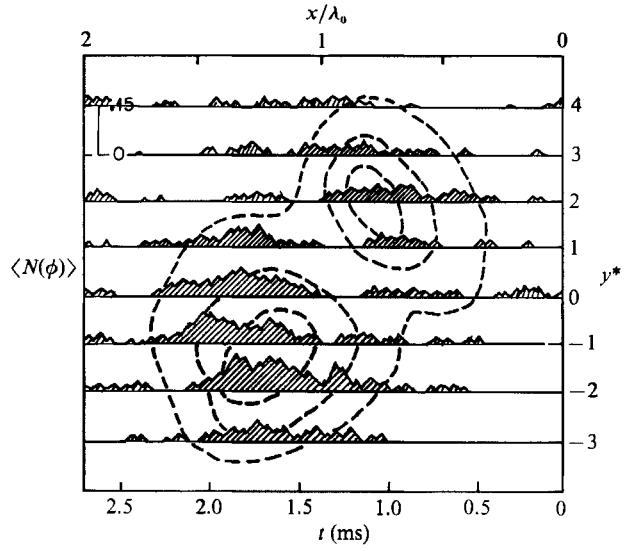

FIGURE 17. Phase average $\langle N\rangle$ over a period at $x^* = 3.85$ and $z = -0.5$ cm. The dotted lines indicate the relative position of the spanwise structures.

A measure of how frequently small eddies occur at an instant is defined as

$$\langle N(\phi)\rangle = \lim_{S\to\infty} \frac{1}{S} \sum_{n=1}^{S} I(\phi + nT), \tag{3}$$

where

$\langle\ \rangle$ denotes phase averaging, ϕ the phase angle in one vortex passing period, S the number of samples, T the local vortex passing period, $I(\ )$ a delta function.

The total number of small eddies in one vortex passing period is

$$N = \int_0^T \langle N(\phi)\rangle \, \mathrm{d}\phi. \tag{4}$$

5.5. *The initial occurrence of small eddies*

By using the PVC technique to survey the flow both in the (x, y)- and (y, z)-planes, we could obtain the concentration of the small eddies in relation to the spanwise and the streamwise structures.

At the initial transition region, $x^* = 3.85$, one component of the time-averaged streamwise vorticity, $\Omega_{x'} = \partial V/\partial z$, is plotted in figure 16. The peaks indicated the core positions of the streamwise vortices. The values of N were also measured. The locations of the peaks of these two curves more or less coincided. This figure provided a quantitative support to the observation of the raw data (figure 14) that the random fine eddies are first detected in the cores of the streamwise vortices.

With the help of the phase-reference from the two-dimensional forcing signal, we can construct the phase-averaged spanwise vorticity contours in the (t, y^*)-plane (dashed-lines in figure 17). By multiplying the average speed with t, the time axis is transferred to the pseudo x-axis. The phase average, $\langle N\rangle$, was plotted along with the vorticity contours (the shaded area in figure 17). The data indicated that the fine eddies were detected more frequently at the high-speed side.

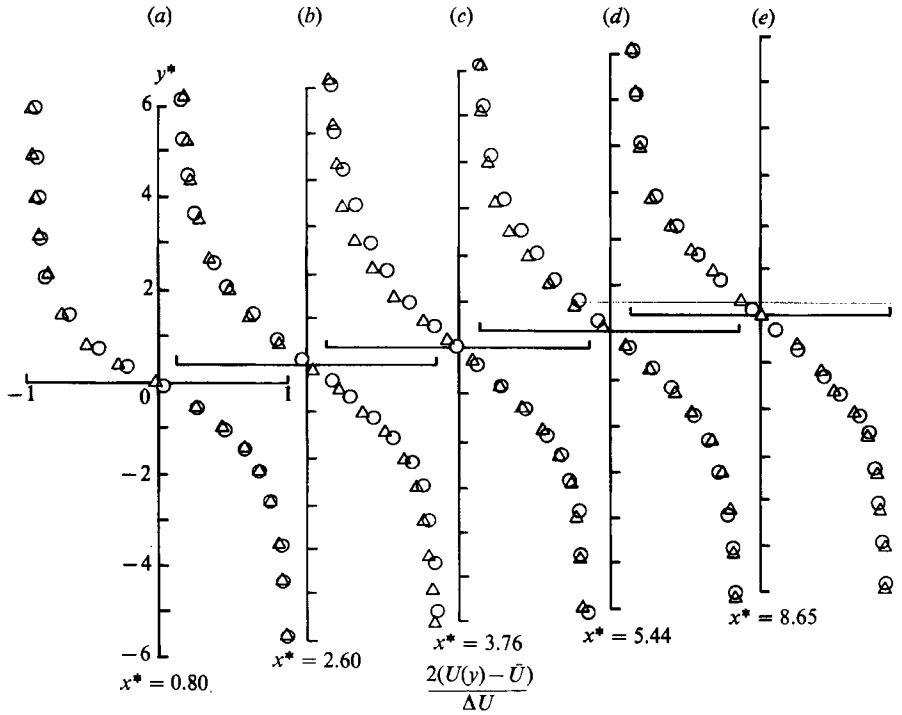

FIGURE 18. Profiles of mean streamwise velocity. △, Unforced case; ○, forced case.

6. Time-averaged flow properties

In this study, velocity ratios and free-stream velocities were varied over a wide range. One of the operating conditions, $U_1 = 19.8$ m/s and $U_2 = 3.63$ m/s, was frequently used for several specific tests. The properties of this flow were measured at mid-span, $z = 0$, and are discussed here.

6.1. *Mean velocity profiles*

The velocity profile measured at the trailing edge of the splitter plate reflected a combination of the wake and the mixing layer. Several lengthscales existed in this type of velocity distribution. Though the wake disappeared within one instability wavelength, the choice of the proper lengthscale was critical in understanding the instability. Zhang, Ho & Monkewitz (1985) examined the stability of a mixing layer forced by the fundamental and subharmonic with different phase angles. They determined that the appropriate initial lengthscale was the thickness of the high-speed shear because it represented most of the vorticity. In the present case, the initial momentum thickness of the high speed shear, θ_0, was 0.95 mm. The measured instability frequency was 750 Hz. Based upon these two values, the Strouhal number, $2\pi f\theta_0/\bar{U}$, was 0.216. This value was close to the stability analysis result based on the tanh profile (Monkewitz & Huerre 1982).

The wake vanished near $x^* = 0.8$ and the mean streamwise velocity distribution became a tanh profile (figure 18). The definition of the momentum thickness is not ambiguous and is defined as

$$\theta = \frac{1}{(\Delta U)^2}\int_{-\infty}^{+\infty}(U_1 - U(y))\,(U(y) - U_2)\,\mathrm{d}y. \tag{5}$$

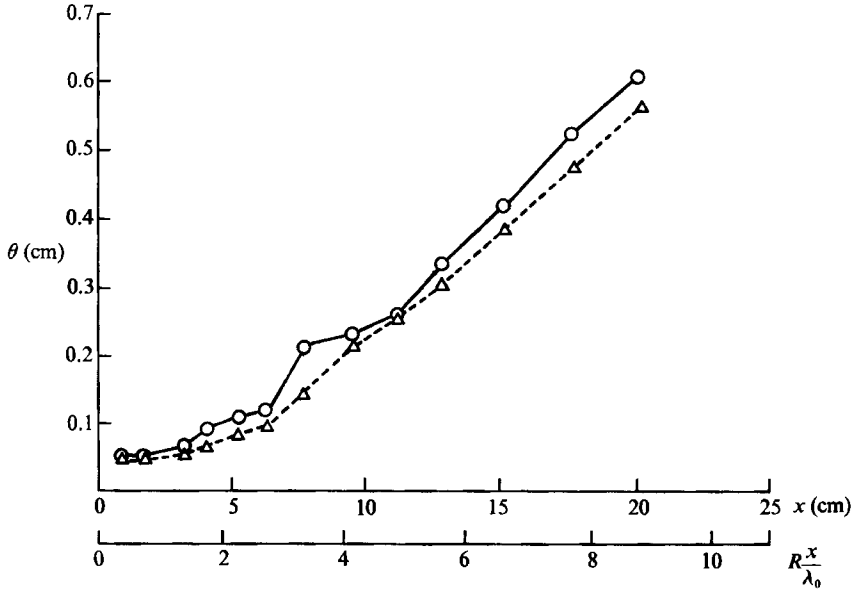

FIGURE 19. Variation of momentum thickness with streamwise distance. △, Unforced case; ○, forced case.

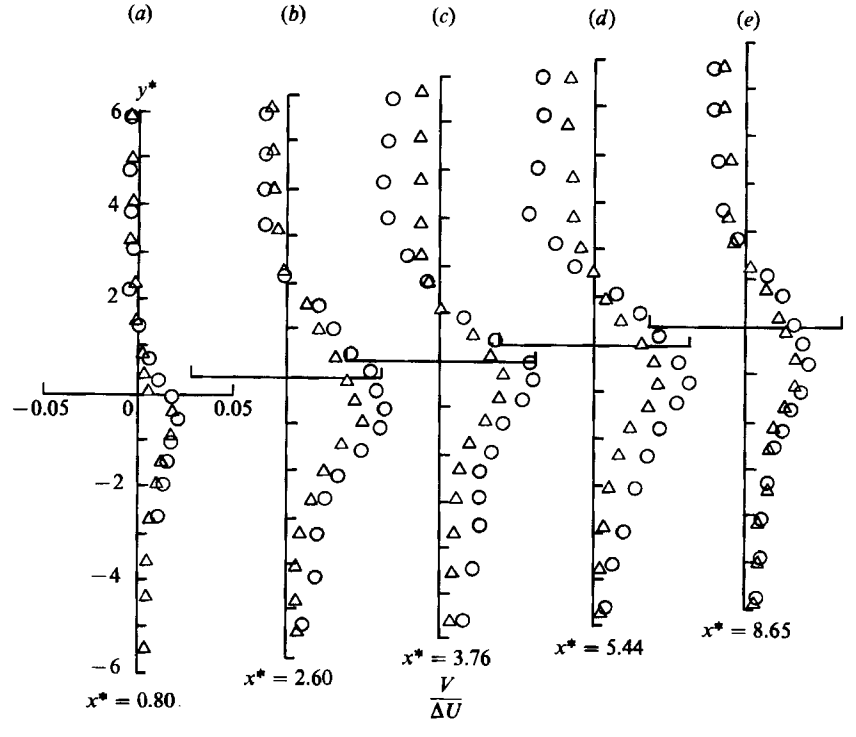

FIGURE 20. Profiles of transverse mean velocity. △, Unforced case; ○, forced case.

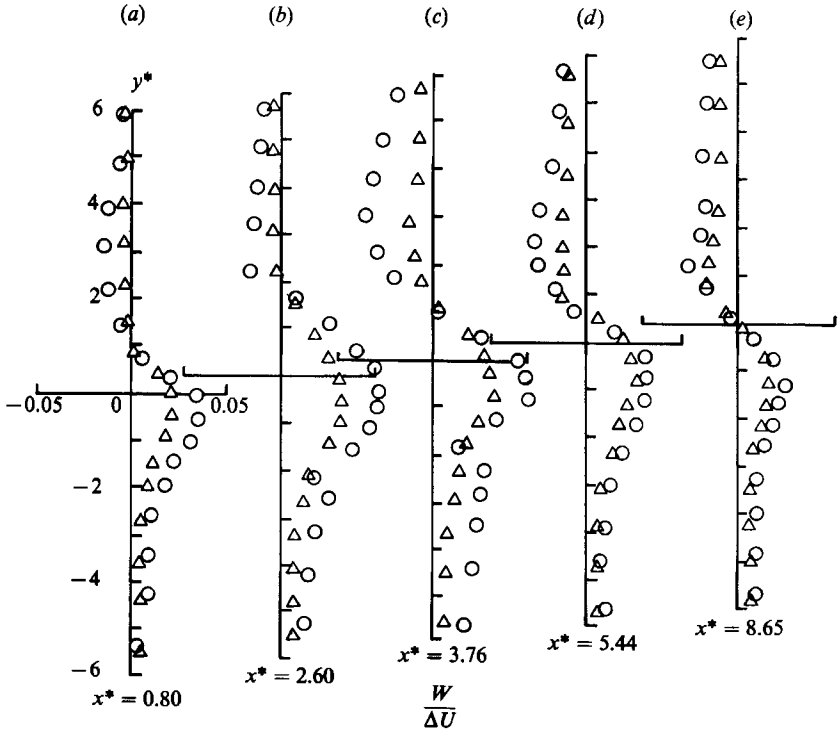

FIGURE 21. Profiles of lateral mean velocity. △, Unforced case; ○, forced case.

The ordinate was normalized with the local momentum thickness. It should be noted that the vorticity thickness, $\delta = \Delta U/(\partial U/\partial y)_{\max}$, was four times the momentum thickness when the flow was laminar and followed the tanh profile (figure 18*a*). The ratio of the vorticity thickness to the momentum thickness increased with distance and reached 5 when the flow became turbulent (figure 18*e*).

The spreading of the mixing layer is shown in figure 19. In the unforced case, the spreading rate was very slow initially and then increased around $x^* = 2$ where the instability waves rolled up into vortices. A greater spreading rate was observed near the vortex merging region, $3 < x^* < 5$. Downstream from this region, the flow started to transition into turbulence and the spreading rate decreased slightly as well as achieved linear growth. The growth of the forced mixing layer was very different from the natural one, it followed the same pattern as was observed in the forced low-Reynolds-number flow (Ho & Huang 1982). Two plateaus, one at the roll-up region and the other at the vortex merging region, existed. The spreading after the second plateau was not quite but close to linear growth, because the second vortex merging location was still more or less localized by the forcing. The Strouhal numbers based upon the local passage frequency and the local thickness at the two plateaus were 0.45, which was close to the neutrally stable frequency. This justified the subharmonic evolution model proposed by Ho (1982).

The time averaged transverse velocity, V, and the lateral velocity, W, are presented in figures 20 and 21. The maximum values of both velocity components were about 5% of the velocity difference, ΔU. Their difference between the forced and unforced cases were not appreciable near the initial region of the mixing layer (figures 20*a* and 21*a*) and in the turbulent region (figures 20*e* and 21*e*). In the vortex

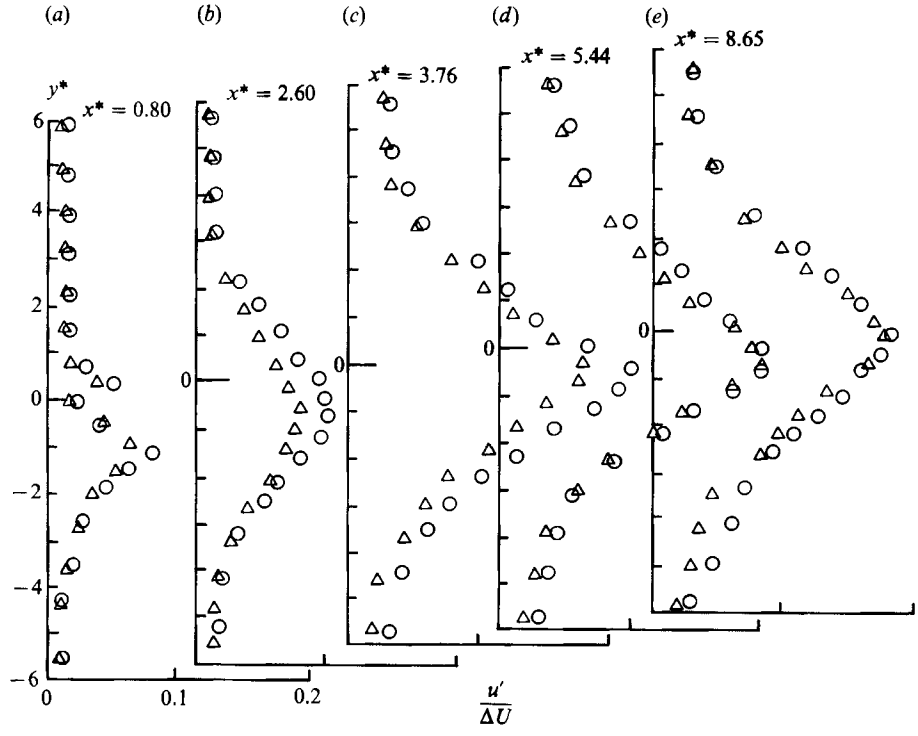

FIGURE 22. Distribution of $u'/\Delta U$. △, Unforced case; ○, forced case.

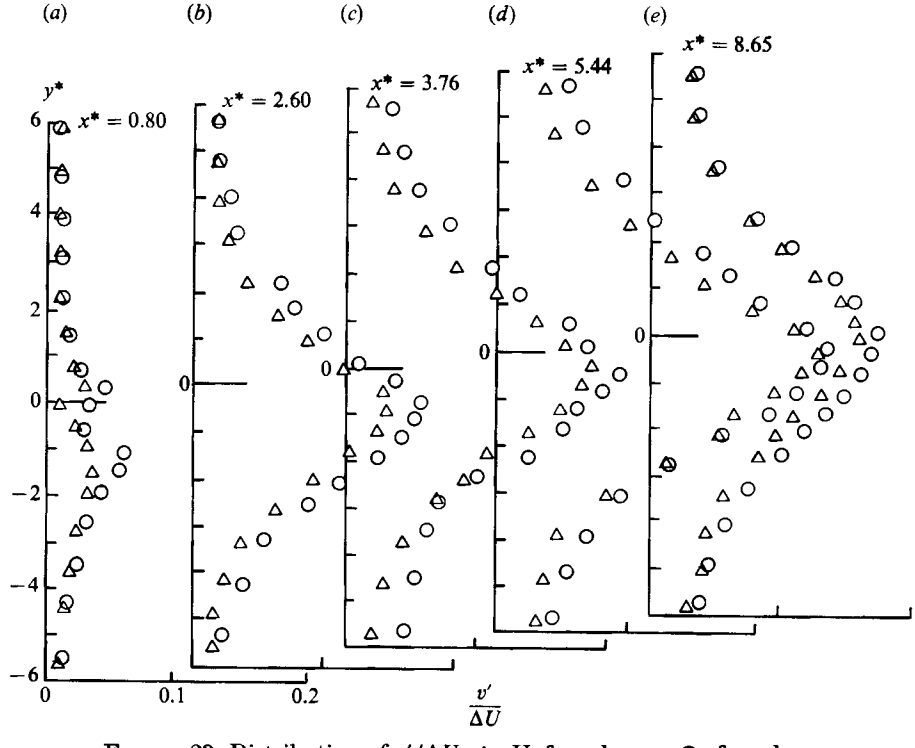

FIGURE 23. Distribution of $v'/\Delta U$. △, Unforced case; ○, forced case.

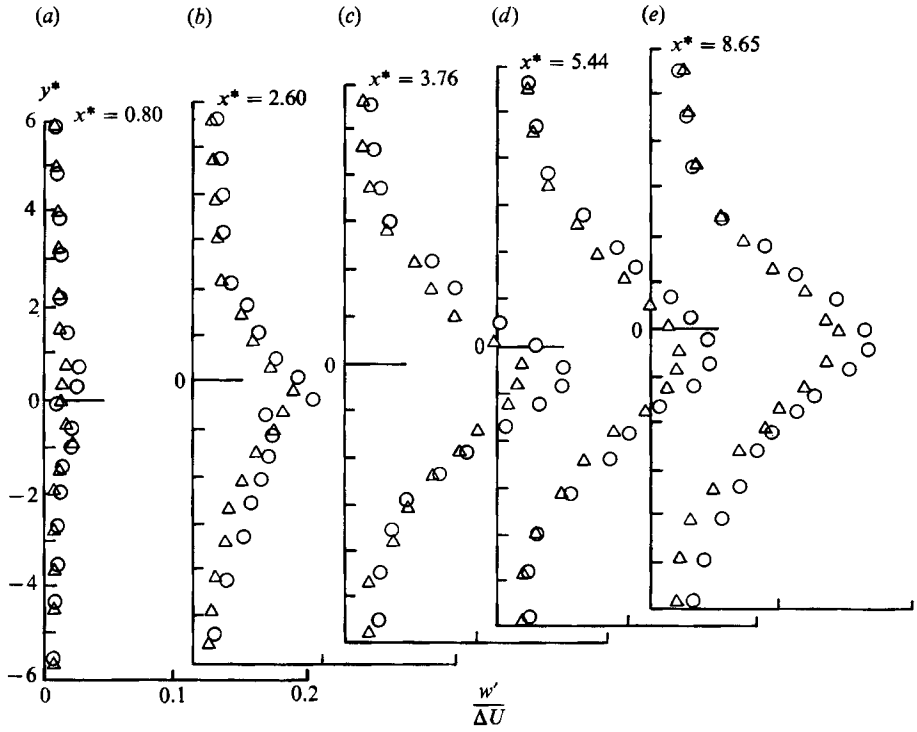

FIGURE 24. Distribution of $w'/\Delta U$. △, Unforced case; ○, forced case.

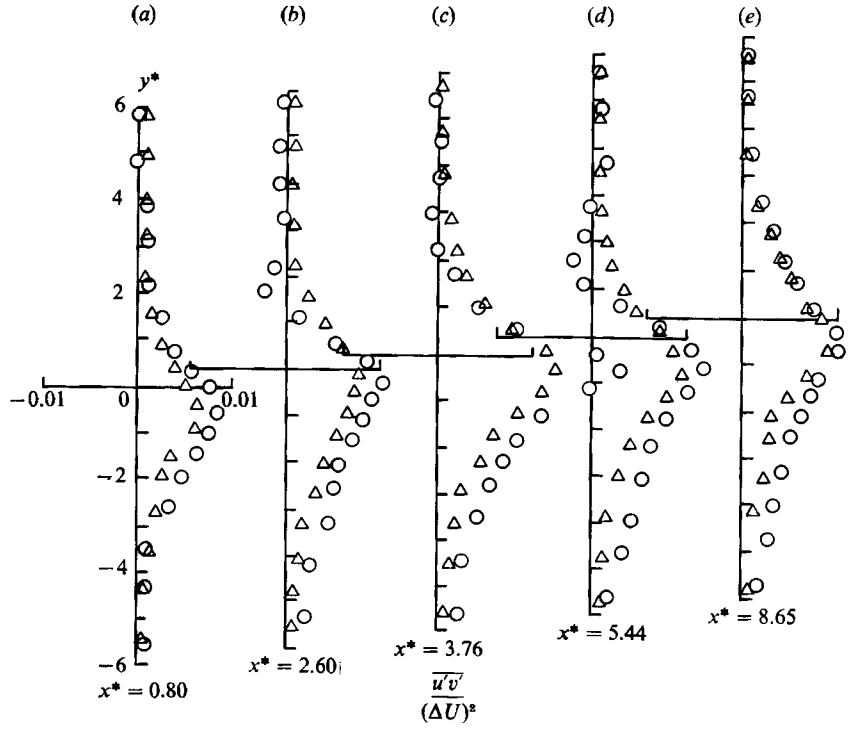

FIGURE 25. Distribution of $\overline{u'v'}/(\Delta U)^2$. △, Unforced case; ○, forced case.

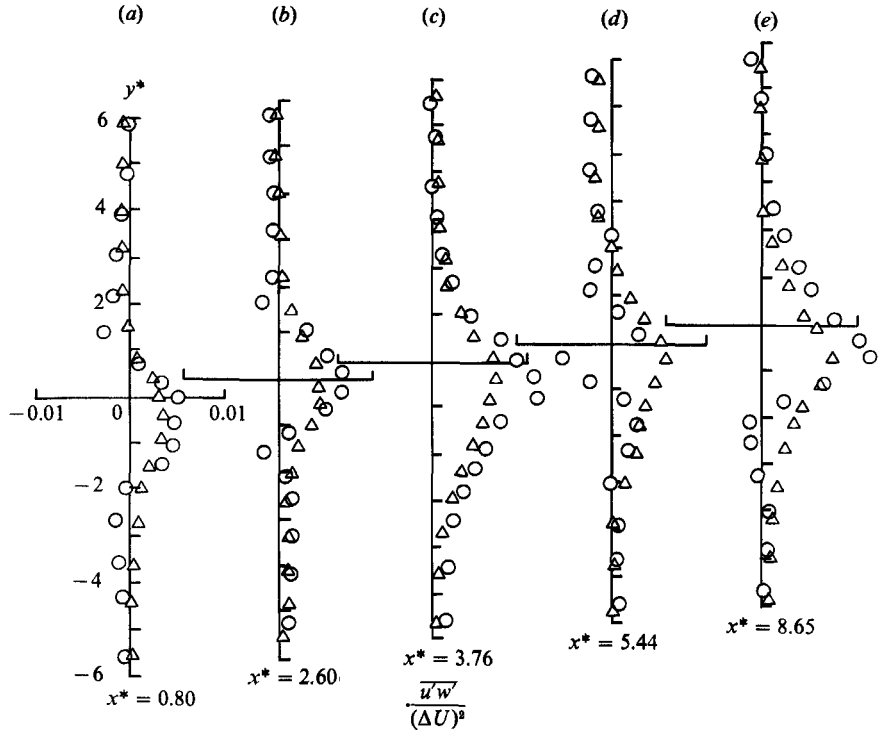

FIGURE 26. Distribution of $\overline{u'w'}/(\Delta U)^2$. △, Unforced case; ○, forced case.

merging region, the transverse velocity in the forced situation was higher than that in the unforced case (figure 20*a–c*), this was a reflection of the high spreading rate for localized vortex merging. The streamwise vortices were localized in the wind tunnel and therefore the time-averaged lateral velocity was non-zero. Under the forced condition, the localized spanwise and streamwise structures produced a dip at $y^* = 2$ (figure 21 b, c). In the natural case, the phase jitter smeared the detailed feature.

6.2. *Fluctuating quantities*

The streamwise velocity fluctuations initially had a double peak distribution (figure 22*a*) and then evolved into a bell-shaped profile (figure 22). The maximum value reached about 20% of ΔU at downstream locations. The fluctuation levels of forced flow in the vortex merging region were slightly higher than that in the unforced case. The spanwise and lateral fluctuating velocities had about the same turbulence levels and were similar to the fluctuating streamwise component (figures 23 and 24).

The maximum Reynolds stress, $\overline{u'v'}$, occurred slightly below the centre of the mixing layer and was about 1% of $(\Delta U)^2$ (figure 25). A small region of negative values (figure 25*b*, *d*) was found at the end of the two plateaus (figure 19). The negative Reynolds stress was due to vortex nutation (Browand & Ho 1983), but it was not as pronounced as that in the strongly forced mixing layer (Oster & Wygnanski 1982). The distributions of the other Reynolds stress component, $\overline{u'w'}$, are shown in figure 26. A dip of the profile was observed at $y^* = 1.5$ for the forced condition (figure 26*b*, *c*). A dip in the mean lateral velocity profile was also found at about the same position (figure 21). Negative Reynolds stress regions were also observed in this figure, but it must be produced by a certain orientation of the streamwise vortices rather than by the spanwise vortex nutation.

7. Conclusions

In a subsonic plane mixing layer, vortex merging is the major mechanism to transfer mass and momentum across the two streams. Vortex merging also increased the wavelengths of the spanwise structures and the streamwise vortices, but the ratio of the two lengthscales was found to be a constant. We further found that the random fine eddies were produced by the interactions of the merging spanwise structures and the streamwise vortices. Therefore, the vortex merging process not only transfers the energy to the subharmonic range, but also shifts the energy to the high-frequency end.

This work is supported by a contract from the Office of Naval Research.

REFERENCES

BERNAL, L. P. 1981 The coherent structure of turbulent layers: I. Similarity of the primary vortex structure. II. Secondary streamwise vortex structure. PhD thesis, Calif. Inst. Technol., Pasadena, CA.

BERNAL, L. P. & ROSHKO, A. 1986 Streamwise vortex structure in plane mixing layers. *J. Fluid Mech.* **170**, 499–525.

BRADSHAW, P. 1966 The effect of initial conditions on the development of a free shear layer. *J. Fluid Mech.* **26**, 225–236.

BREIDENTHAL, R. 1981 Structure in turbulent mixing layers and wakes using a chemical reaction. *J. Fluid Mech.* **109**, 1–24.

BROWAND, F. K. & HO, C. M. 1983 The mixing layer: an example of quasi two-dimensional turbulence. *J. Mech. Theor. Appl. Special Suppl.*, pp. 99–120.

BROWAND, F. K. & LATIGO, B. O. 1979 Growth of the two-dimensional mixing layer from a turbulent and non-turbulent boundary layer. *Phys. Fluids* **64**, 775–816.

BROWN, G. L. & ROSHKO, A. 1974 On density effects and large structure in turbulent mixing layers. *J. Fluid Mech.* **64**, 775–816.

BURG, J. P. 1967 Maximum entropy spectral analysis. Presented at the 37th Ann. Intl Meeting, Soc. of Explo. Geophys., Oklahoma City, Oklahoma.

CHEN, W. Y. & STEGEN, G. R. 1974 Experiments with maximum entropy power spectra of sinusoids. *J. Geophys. Res.* **79**, 3019–3022.

CORCOS, G. M. & LIN, S. J. 1984 The mixing layer: deterministic models of a turbulent flow. Part 2. The origin of the three-dimensional motion. *J. Fluid Mech.* **139**, 67–95.

FIEDLER, H. E. & MENSING, P. 1985 The plane turbulent shear layer with periodic excitation. *J. Fluid Mech.* **150**, 281–309.

HO, C. M. 1982 Local and global dynamics of free shear layers. In *Numerical and Physical Aspects of Aerodynamic Flows* (ed. T. Cebeci), pp. 521–533. Springer.

HO, C. M. & GUTMARK, E. 1987 Vortex induction and mass entrainment in a small-aspect-ratio elliptic jet. *J. Fluid Mech.* **179**, 383–405.

HO, C. M. & HUANG, L. S. 1982 Subharmonics and vortex merging in mixing layers. *J. Fluid Mech.* **119**, 443–473.

HO, C. M. & HUERRE, P. 1984 Perturbed free shear layers. *Ann. Rev. Fluid Mech.* **16**, 365–424.

HSIAO, F. B. 1985 Small scale transition and preferred mode in an initially laminar plane jet. PhD thesis, University of Southern California, Los Angeles, CA.

HUANG, L. S. 1985 Small scale transition in a two-dimensional mixing layer. PhD thesis, University of Southern California, Los Angeles, CA.

JIMENEZ, J. 1983 A spanwise structure in the plane shear layer. *J. Fluid Mech.* **132**, 319–336.

JIMENEZ, J., MARTINEZ-VAL, R. & REBOLLO, M. 1979 On the origin and evolution of three-dimensional effects in the mixing layer. *Intern. Rep.* DA-ERO-70-G-079, Univ. Politec. Madrid, Spain.

KONRAD, J. H. 1976 An experimental investigation of mixing in two-dimensional turbulent shear flows with applications to diffusion-limited chemical reactions. *Intern. Rep.* CIT-8-PU, Calif. Inst. Technol. Pasadena, CA.

LASHERAS, J. C., CHO, J. S. & MAXWORTHY, T. 1986 On the origin and scale of streamwise vortical structures in a plane, free shear layer. *J. Fluid Mech.* **172**, 231–258.

LEE, M. & REYNOLDS, W. C. 1985 Bifurcating and blooming jet. *Tech. Rep.* TF-22. Stanford University.

LESIEUR, M., STAQUET, C., LE ROY, P. & COMTE, P. 1988 The mixing layer and its coherence examined from the point of view of two-dimensional turbulence. *J. Fluid Mech.* **192**, 511–534.

LIU, J. T. C. 1986 Contributions to the understanding of large-scale coherent structures in developing free turbulent shear flows. *Adv. Appl. Mech.* **26**, 183–309.

LIU, J. T. C. & MERKINE, L. 1976 On the interactions between large-scale structure and fine-grained turbulence in a free shear flow. *Proc. R. Soc. Lond.* A **352**, 213–247.

METCALFE, R. W., ORSZAG, S. A., BRACHET, M. E., MENON, S. & RILEY, J. J. 1987 Secondary instability of a temporally growing mixing layer. *J. Fluid Mech.* **184**, 207–243.

MIKSAD, R. W. 1972 Experiments on the nonlinear stages of free-shear-layer transition. *J. Fluid Mech.* **56**, 695–719.

MONKEWITZ, P. A. & HUERRE, P. 1982 The influence of the velocity ratio on the spatial instability of mixing layers. *Phys. Fluids* **25**, 1137–1143.

NYGAARD, K. J. & GLEZER, A. 1988 Spanwise nonuniformly forced plane mixing layer. *Bull. Am. Phys. Soc.* **33**, 2297.

OSTER, D. & WYGNANSKI, I. 1982 The forced mixing layer between parallel streams. *J. Fluid Mech.* **123**, 91–130.

PIERREHUMBERT, R. T. & WIDNALL, S. E. 1982 The two- and three-dimensional instabilities of a spatially periodic shear layer. *J. Fluid Mech.* **114**, 59–82.

RILEY, J. J. & METCALFE, R. W. 1980 Direct numerical simulation of a perturbed, turbulent mixing layer. *AIAA paper*, no. 80-0274.

ROBINSON, A. C. & SAFFMAN, P. G. 1984 Three-dimensional stability of an elliptical vortex in a straining field. *J. Fluid Mech.* **142**, 451–466.

SATO, H. 1960 The stability and transition of a two-dimensional jet. *J. Fluid Mech.* **7**, 53–80.

TUKEY, J. W. 1974 Nonlinear (nonsuperposable) methods for smoothing data. In *Cong. Rec. EASCON*, p. 673.

WINANT, C. D. & BROWAND, F. K. 1974 Vortex pairing: the mechanism of turbulent mixing layer growth at moderate Reynolds number. *J. Fluid Mech.* **63**, 237–255.

WYGNANSKI, I. & PETERSEN, R. A. 1985 Coherent motion in excited free shear flows. *AIAA paper*, no. 85-0539.

ZHANG, Y. Q., HO, C. M. & MONKEWITZ, P. A. 1985 The mixing layer forced by fundamental and subharmonic. *Proc. of 2nd IUTAM Symposium Laminar–Turbulent Transition, Novosibirsk, USSR.* pp. 385–395. Springer.

ZOHAR, Y., FOSS, J. & HO, C. M. 1987 Phase decorrelation of coherent structures in mixing layers. *Bull. Am. Phys. Soc.* **32**, 2048.

ZOHAR, Y., HO, C. M., MOSER, R. & ROGERS, M. M. 1988 Evolution of streamwise vortices in mixing layers. *Bull. Am. Phys. Soc.* **33**, 2255.